Supporting Information for

Short and Long-range cyclic patterns in flows of DNA solutions in microfluidic obstacle arrays

Oskar E. Ström, Jason P. Beech, Jonas O. Tegenfeldt(*)

Division of Solid State Physics, Department of Physics, Lund University

NanoLund, Lund University.

*Jonas O. Tegenfeldt.

Email: jonas.tegenfeldt@ftf.lth.se

This PDF file includes:

Supporting text

Figures S1 to S5

SI References

Other supporting information for this manuscript include the following:

Movies S1 to S7

1. Addition of sucrose to the DNA sample - Boger fluid

To explore the effect of shear thinning, we prepare a Boger fluid, a fluid with elastic properties but without shear thinning. Figure S1 shows clearly that the added sucrose results in wave formation with a DNA concentration that would otherwise be insufficient.

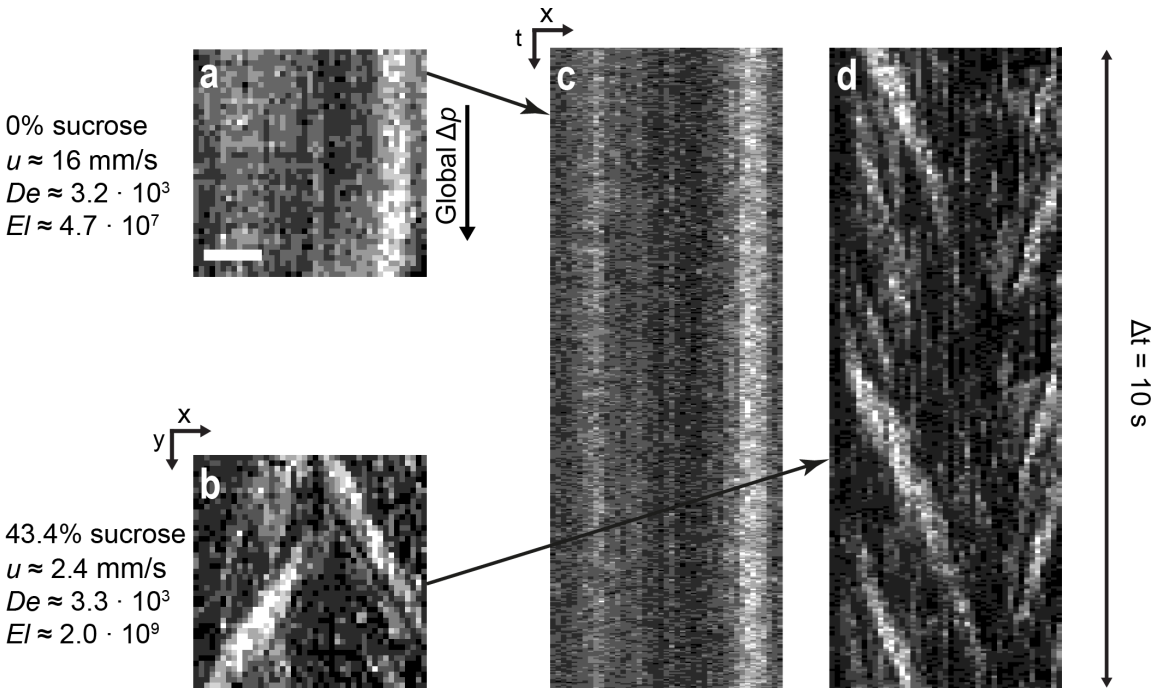

Fig. S1. Low DNA concentrations (50 µg/mL, C/C* = 0.43, λ DNA) without (a, c) and with (b, d) added sucrose (w/w %) in the quadratic array. (a) and (b) show snapshots or arrays (pillars removed by image processing, see materials and methods). (c) and (d) show the corresponding kymographs at the middlemost row (y direction) with the same horizontal spatial scale (x direction). The zero-shear viscosity of the sample with sucrose is approximately four times higher than that without (6.5 mPas and 1.9 mPas respectively, based on data from [1] and [2]). The infinite-shear viscosity is however about 5.4× higher as the viscosity of DNA solutions have been shown to approach the solvent viscosity at very high shear rates [1]. The spatial scales are identical for all images with the scale bar representing 200 µm.

2. Calculation of the overlap concentration and the ionic strength

The overlap concentration [3] is given by $C^* = M/[(4\pi/3)R_g^3 N_A]$. Here, M is the molecular weight of the DNA and N_A is Avogadro's number. C^* is the concentration above which DNA molecules no longer behave like isolated, individual molecules. Together with the expression for the radius of the polymer below, we obtain an expression for C^* that depends on the contour length, L, as $C^* \propto L^{(1-3\nu)} \approx L^{-0.8}$, where ν is the Flory exponent, $\nu = 0.5877$ [4]. Fig. S2 shows the relationship of the overlap concentration with I and L. We illustrate the dependence of the overlap concentration on ionic strength and on molecular length in Fig. S2.

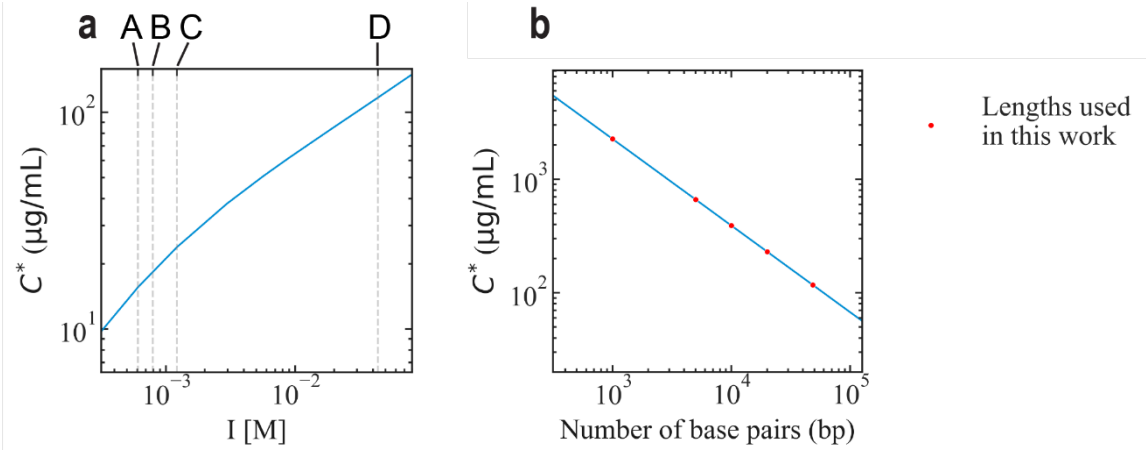

Fig. S2. The dependence of the overlap concentration, C^*, on the ionic strength for λ DNA (a) and the number of base pairs of the DNA (b) at high salt (5× TE, 3% BME). Values are based on T = 22 °C and with a dye to base pair ratio of 1:200. The buffer concentrations used for our work are indicated by the dashed vertical lines in (a) as 0.1× TE, 0.13× TE, 0.2× TE, and 5× TE and 3% BME for A-D, respectively. The lengths of the DNA used for our work are highlighted using red dots in (b).

The radius of gyration, R_g, used in our calculations for C^* is estimated using the worm-like chain (WLC) model (also known as the Kratky-Porod model) as $R_g \approx R_e/\sqrt{6}$, where R_e is the polymer end-end distance. To make the estimate as accurate as possible, electrostatic interactions and excluded volume effects are taken into account. R_e is then described as [5]:

$$R_e \approx \left(w_{eff} l_p\right)^{1/5} (bN)^{\nu} \qquad [1]$$

where w_{eff} is the effective width of the polymer, l_p is the persistence length, $b = 2l_p$ is the Kuhn length and N is the number of Kuhn segments, $N = L/b$, where L is the contour length. For every dye molecule incorporated into the DNA strand, the contour length is increased by 0.51 nm [6]. l_p depends on ionic strength according to Odijk–Skolnick–Fixman (OSF) theory[7-9] as:

$$l_p = l_p' + \frac{0.0324\text{M}}{I}\ \text{nm} \qquad [2]$$

where $l_p' = 50$ nm is the bare persistence length and I is the ionic strength of the buffer. See below for how we calculated I for the different buffers used.

The effective width for strongly charged chains, such as DNA, is given by [5]:

$$w_{eff} = \frac{1}{\kappa}\left[0.7704 + log\left(\frac{\nu_{eff}^2}{2\varepsilon\varepsilon_0 k_b T\kappa}\right)\right] \qquad [3]$$

where $1/\kappa$ is the Debye length, ϵ the dielectric constant of water, ε_0 the permittivity of free space, ν_{eff} is the effective DNA line charge density, k_B is Boltzman's constant and T the temperature. We use $\nu_{eff} = -0.593\ e/\text{Å}$ [10], where e is the elementary charge. For a buffer containing 5× TE and 3% BME (I = 44 mM) at T = 22 °C we calculate $w_{eff} = 4.6$ nm and

for a buffer of 1× TE at the same T, $w_{eff} = 43$ nm which corresponds well with literature values from Iarko *et al.* [11].

The Ionic strength, *I*, is calculated by summing the product of the concentration and squared charge of all ions in the solution:

$$I = \frac{1}{2}\sum_{i=0}^{n} z_i^2 c_i \qquad [4]$$

where the one half is added to include both anions and cations and c_i is the concentration of an ionic species with the valence z_i. We use the python library SymPy to compute *I* based on the detailed description by Iarko *et al.* [11]. The equilibrium concentrations are calculated by solving a series of equations consisting of the equilibrium conditions based on the law of mass action. The activity coefficients of these conditions are calculated using the Davis equation. Because the activity coefficient depends on the ionic strength which in turn depends on the activity coefficients, the system of equations is iterated until a stable solution is found. The initial activity coefficients are set to 1. The percent error (100 × [calculated value – literature value] / literature value) is below 0.6% [12].

3. Calculations of various dimensionless numbers

Dimensionless numbers are used extensively in our description of our work. However, it is important to be aware that they vary across the devices that we use both in space and in time. The main purpose is to give an overall idea of the nominal properties of the fluids and what factors influence the behavior of the fluids in the devices.

The Reynolds number describes the relationship between inertial effects and viscous effects, and is calculated according to $Re \equiv \rho \cdot u \cdot w/\eta_s$,where u is the mean fluid velocity in the pillar gaps of the array, w is the gap width between the pillars, ρ is the fluid density and η_s is the solvent viscosity. In our case we have $Re << 1$ and thus we can treat any inertial effects as negligible.

The Deborah number, *De,* describes the ratio between the relaxation time of the system (here the DNA molecules) and the time scale of the applied forces (here the interaction time between the flowing molecules and individual pillars) [13]. In the present work, we define $De \equiv (u/L_{pp})\tau_Z$, where, L_{pp} is the center-to-center distance between array rows and τ_Z is the Zimm relaxation time of the polymer. Note that τ_Z only gives approximate values of the relaxation time as it assumes the conditions to be ideal, the solution to be dilute and the solution to be in equilibrium.

We define the elasticity number, $El = De/Re$, which describes the ratio of elastic stress to inertial stress, with the Deborah number rather than the Weissenberg number since the shear rate in our system is not constant along the channel.

We estimate the relaxation time, τ_z, using the Zimm relaxation time [14], $\tau_{Zimm} = R_g^2/D_Z \approx \eta_s\, b^3 N^{3\nu}/(k_B T) \propto L^{3\nu} \propto L^{1.76}$ where η_s is the solvent viscosity, *b* is the Kuhn length, k_B is Boltzmann's constant, *T* is temperature, *N* is the number of Kuhn segments and ν is the

Flory exponent. In the semidilute regime, the equilibrium relaxation time can be expressed in terms of the ratio between the concentration and the overlap concentration [15]:

$$\tau \propto (C/C^*)^{(2-3\nu)/(3\nu-1))} \approx (C/C^*)^{0.31}.$$

The magnitudes of the dimensionless numbers presented in the main text should be considered lower bounds. Based on data from [16-19] we can estimate that the relaxation time and thus our estimates for *De* and *El* can be increased by at least a factor of 3 for $C \approx 4C^*$ with concentrated λ DNA samples and a factor of 30 for the concentrated T4 DNA sample ($C \approx 9C^*$). The shear thinning has a two-fold decreasing effect on *El* as both the viscosity [1,17] and the relaxation time [20] have been shown to reduce with higher shear rates. We would ultimately expect *El* to be significantly higher than reported in this work at high *C* and low flow velocities and slightly lower at high flow velocities.

Table S1. Comparison of polymer weight and concentration between Pluronic® and λ DNA.

Polymer	Polymer weight (MDa)	*C* (μg/mL)	*C* (% w/w)
Pluronic® F-127 (poloxamer 407)	0.012	10	0.001%
lambda phage DNA (λ DNA, 48.5 kbp)	31.5	400	0.04%

Table S2. Weight and concentration ratios between λ DNA and Pluronic®.

Weight Ratio(λ DNA/Pluronic®)	Concentration Ratio (λ DNA/Pluronic®)
2522	39.98

4. Rheology measurements

The relaxation time of a solution of 400 μg/mL lambda phage DNA in 5× TE buffer was measured using a stress-controlled rheometer (Physica MCR 301, Anton Paar) with a 25 mm cone plate geometry (CP 25-1) at 25 °C. An amplitude measurement was performed to find the linear viscoelastic (LVE) region, Fig. S3, and 30% of the maximum strain was chosen for subsequent frequency measurements. Three measurement series were taken and the means of G' and G'' used to find the cross-over frequency, at which the relaxation time τ is equal to the inverse of the angular frequency. This gave a value for the relaxation time of 1.43 s, Fig. S4, S5. This relaxation time is within the same order of magnitude as the calculated Zimm relaxation time for the same solution (2.6 s, see Table 1 in the main text).

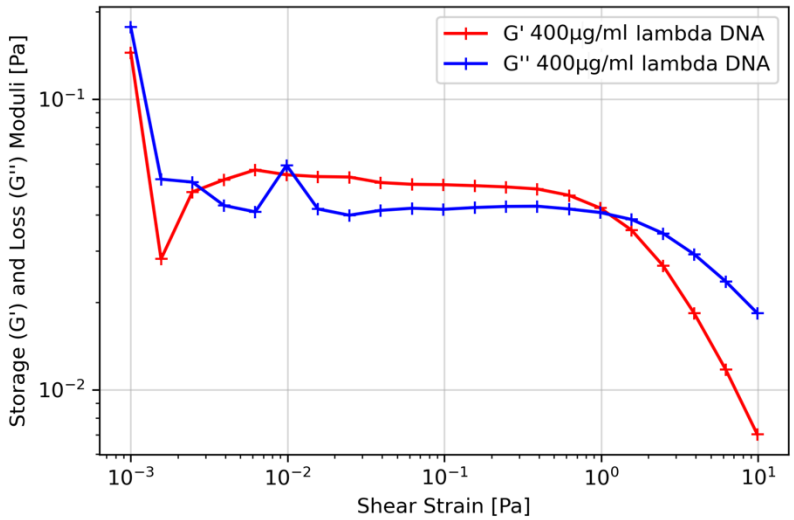

Fig. S3. Amplitude sweep to determine the linear viscoelastic (LVE) region.

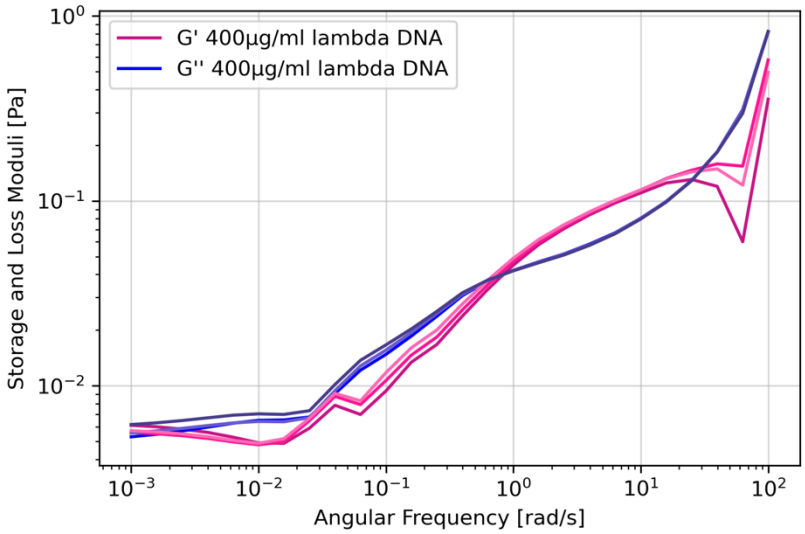

Fig. S4. Frequency sweeps (triplicate) for a solution of 400 µg/mL λ DNA in 5× TE buffer.

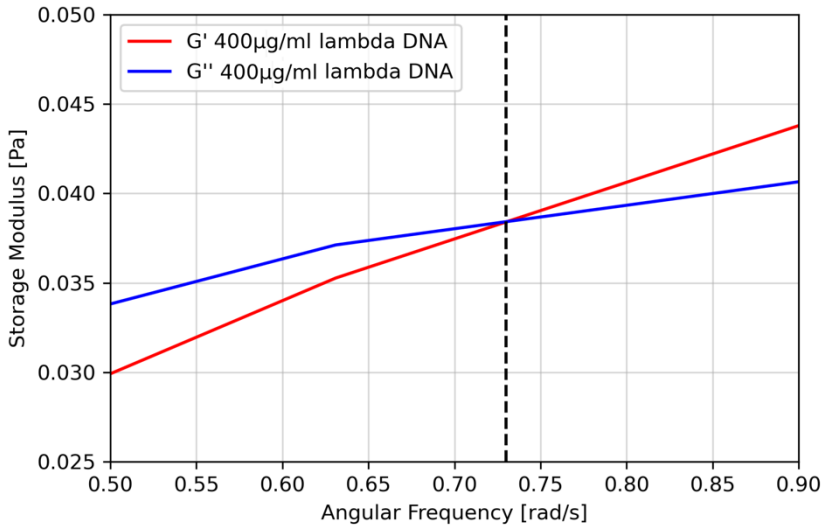

Fig. S5. The average of the three frequency sweeps from Fig. S4. The relaxation time is derived from the cross-over frequency where G' = G'' which is shown with the black, vertical dashed line.

5. Movies

Movie S1. (separate file). Low-magnification (2×) videographs comparing low flow velocity ($u \approx 10^2$ μm/s, $De \approx 10^2$) to high flow velocity ($u \approx 10^3$ μm/s, $De \approx 10^3$) of λ DNA solutions flowing through quadratic and disordered arrays. The Movie contains data that corresponds to Fig. 1.

Movie S2. (separate file). Low-magnification (4×) fluorescence videographs where Δp is ramped from no flow to high flow rate ($De \approx 10^3$) with a λ DNA solution of $C = 400$ μg/mL and high salt ($I = 44$ mM). Data for quadratic array.

Movie S3. (separate file). High-magnification (20×) videographs of the three flow regimes S, C and W with a λ DNA solution of high $C = 400$ μg/mL and high salt ($I = 31$ mM). Note that the video playback rate is set the same for all flow velocities, so that the higher flow velocity video sections are slowed down. Data for quadratic array. The Movie contains data that corresponds to Fig. 2 and 3.

Movie S4a. (separate file). Low-magnification (10×) fluorescence videographs of low $C = 50$ μg/mL and high $C = 400$ μg/mL λ DNA solution, at high flow rate ($De \approx 10^3$) and high salt ($I = 44$ mM). Data for quadratic array.

Movie S4b. (separate file). Low-magnification (10×) fluorescence videographs (where the pillars have been removed) of low $C = 50$ μg/mL and high $C = 400$ μg/mL λ DNA solution, at high flow rate ($De \approx 10^3$) and high salt ($I = 44$ mM). Data for quadratic array.

Movie S5. (separate file). Low-magnification (4×) fluorescence videograph sweeping the field of view across the entire array for a λ DNA solution of low salt ($I = 1.2$ mM) and $C = 50$ μg/mL, high flow rate ($De \approx 10^3$). Data for quadratic array.

Movie S6. (separate file). High-magnification (100×) videographs of low ($De \approx 26$) and high flow rates ($De \approx 1.1 \times 10^3$) for a λ DNA solution of high $C = 400$ μg/mL and high salt ($I = 44$ mM). Note that the color represents the polarization emission ratio and the pixel value the total fluorescence intensity. Data for quadratic array. The Movie contains data that corresponds to Fig. 4.

Movie S7. (separate file). Low-magnification (10×) videographs of low ($De \approx 26$) and high ($De \approx 1.1 \times 10^3$) flow rates for a λ DNA solution of high $C = 400$ μg/mL and high salt ($I = 44$ mM). The pillars have been removed with image processing and each pixel represents the average value of a dead zone. Note that the color represents the polarization emission ratio and the pixel value the total fluorescence intensity. Data for quadratic array. The Movie contains data that corresponds to Fig. 4.

6. References

1 Dakhil, H. *et al.* Buffered λ-DNA solutions at high shear rates. *Journal of Rheology* **65**, 159-169 (2021).

2 Telis, V. R. N., Telis-Romero, J., Mazzotti, H. & Gabas, A. L. Viscosity of aqueous carbohydrate solutions at different temperatures and concentrations. *International Journal of food properties* **10**, 185-195 (2007).

3 Doi, M. & Edwards, S. F. *The theory of polymer dynamics*. Vol. 73 (Oxford university press, 1988).

4 Li, B., Madras, N. & Sokal, A. D. Critical exponents, hyperscaling, and universal amplitude ratios for two-and three-dimensional self-avoiding walks. *Journal of Statistical Physics* **80**, 661-754 (1995).

5 Reisner, W., Pedersen, J. N. & Austin, R. H. DNA confinement in nanochannels: Physics and biological applications. *Reports on Progress in Physics* **75**, doi:10.1088/0034-4885/75/10/106601 (2012).

6 Günther, K., Mertig, M. & Seidel, R. Mechanical and structural properties of YOYO-1 complexed DNA. *Nucleic Acids Research* **38**, 6526-6532, doi:10.1093/nar/gkq434 (2010).

7 Odijk, T. Polyelectrolytes near the rod limit. *Journal of Polymer Science: Polymer Physics Edition* **15**, 477-483 (1977).

8 Skolnick, J. & Fixman, M. Electrostatic persistence length of a wormlike polyelectrolyte. *Macromolecules* **10**, 944-948 (1977).

9 Dobrynin, A. V. Effect of counterion condensation on rigidity of semiflexible polyelectrolytes. *Macromolecules* **39**, 9519-9527 (2006).

10 Stigter, D. Wall effects on DNA stretch and relaxation. *Biophysical chemistry* **101**, 447-459 (2002).

11 Iarko, V. *et al.* Extension of nanoconfined DNA: Quantitative comparison between experiment and theory. *Physical Review E - Statistical, Nonlinear, and Soft Matter Physics* **92**, 1-8, doi:10.1103/PhysRevE.92.062701 (2015).

12 Hsieh, C.-c., Balducci, A. & Doyle, P. S. Ionic Effects on the Equilibrium Dynamics of DNA Confined in Nanoslits. **3**, 2-7 (2008).

13 Ekanem, E. M., Berg, S., De, S., Fadili, A. & Luckham, P. Towards Predicting the Onset of Elastic Turbulence in Complex Geometries. *Transport in Porous Media* **143**, 151-168, doi:10.1007/s11242-022-01790-8 (2022).

14 Rubinstein, M. & Colby, R. H. *Polymer physics*. Vol. 23 (Oxford university press New York, 2003).
15 Rouse Jr, P. E. A theory of the linear viscoelastic properties of dilute solutions of coiling polymers. *The Journal of Chemical Physics* **21**, 1272-1280 (1953).
16 Teixeira, R. E., Dambal, A. K., Richter, D. H., Shaqfeh, E. S. & Chu, S. The individualistic dynamics of entangled DNA in solution. *Macromolecules* **40**, 2461-2476 (2007).
17 Pan, S., At Nguyen, D., Sridhar, T., Sunthar, P. & Ravi Prakash, J. Universal solvent quality crossover of the zero shear rate viscosity of semidilute DNA solutions. *Journal of Rheology* **58**, 339-368 (2014).
18 Gong, Z. & van der Maarel, J. R. Translational and reorientational dynamics of entangled DNA. *Macromolecules* **47**, 7230-7237 (2014).
19 Hsiao, K.-W., Sasmal, C., Ravi Prakash, J. & Schroeder, C. M. Direct observation of DNA dynamics in semidilute solutions in extensional flow. *Journal of Rheology* **61**, 151-167 (2017).
20 Huang, C.-C., Gompper, G. & Winkler, R. G. Non-equilibrium relaxation and tumbling times of polymers in semidilute solution. *Journal of Physics: Condensed Matter* **24**, 284131 (2012).